Cooperative Task and Motion Planning for Multi-Arm Assembly Systems

Jingkai Chen[1], Jiaoyang Li[2,*], Yijiang Huang[1,*], Caelan Garrett[1,4], Dawei Sun[3],
Chuchu Fan[1], Andreas Hofmann[1], Caitlin Mueller[1], Sven Koenig[2], Brian C. Williams[1]

***Abstract*—Planning for a team of robots to complete varying assembly tasks in dynamic environments is one of the key technical challenges for developing the next generation of manufacturing automation. In this paper, we present a cooperative task and motion planning framework that jointly plans safe, optimized assembly plans for multiple robot arms to assemble complex spatial structures. We demonstrate our planning system on several challenging domains including Lego bricks, bars, plates, and irregular-shaped blocks with up to three robots with grippers or suction plates for assembling up to 23 objects. We show that, with our framework, assembly plans can be automatically planned for various complex structures and potentially applied to real-world manufacturing.**

I. Introduction

As automated assembly lines were one of the earliest applications of robotics since the 1960s, the number of robots deployed for repetitive assembly tasks in factories has been significantly increased in the past decades. However, most robotic assembly automation is manually designed by professional engineers and usually takes months to accommodate new production needs. In the coming generation, robotic assembly automation is expected to be more adaptable to changing environments and flexible assembly requirements. This calls for automating robotic assembly automation with robotic task and motion planning with respect to varying machine setups and products.

Existing methods are nowhere close to automating the above process. There are four open challenges in task and motion planning for generating assembly plans: (1) *planning for high-dimensional manipulators:* industrial robot manipulators typically have more than six degrees of freedom (DOFs). Due to the presence of both static obstacles and dynamic obstacles (e.g., moving robots and assembled parts), planning collision-free motions and manipulation plans for such high-dimensional systems is computationally challenging; (2) *planning over a long horizon:* assembly requirements in manufacturing typically include a large number of different tasks (e.g., assembling, holding, and welding) over a long horizon, and these tasks are often tightly coupled with precedence constraints and concurrency requirements given the product properties. These requirements complicate the planning problem with a longer planning horizon and non-negligible dependency between motion plans across different tasks; (3) *cooperative planning for heterogeneous robot teams:* deploying multiple robots with different tools in manufacturing is not only critical to increasing assembly productivity but also provides the ability to assemble more complex products via cooperation. Planning with such a cooperative robot team significantly increases the problem dimension; (4) *optimizing assembly time:* optimizing the makespan (i.e., total assembly time) is critical for industrial applications. Finding such an optimal or near-optimal solution for the multi-task, multi-robot assembly planning problem requires thorough consideration over all the aspects mentioned above.

Consider the example in Fig. 1. Two robot arms R1 and R2 must detach and attach the bricks to move them from their start configurations to their goal configurations (see top left). The assembly task plan is given in the bottom left of Fig. 1. In particular, after the blue brick (B) is assembled in its goal configuration, one robot needs to hold B in order for the other robot to attach the red brick (R) (see Steps 4 and 5 in bottom right of Fig. 1). One needs to assign these tasks to the two robot arms (see the assignment in the top right of Fig. 1) and plan paths that adhere to the assignments while avoiding three types of collisions (see the bottom middle of Fig. 1). The bottom right sketches an optimized collision-free assembly plan with six critical moves.

We propose a cooperative task and motion planning framework to plan optimized assembly plans for multi-task multi-robot assembly problems, which addresses the above challenges. The framework structure is shown in Fig. 1. This planning system takes as input the robot and assembly structure setup along with descriptions of the possible robot operating modalities, called mode graphs, and goal descriptions, called assembly task plans. The planning system consists of three phases: (1) generate a multi-modal roadmap for each robot that describes its feasible movements and interactions with objects and annotate the colliding situations among the different roadmaps (2) optimally assign assembly tasks to robots with respect to their roadmaps by using Mixed Integer-Linear Programs (MILPs), in which we temporarily ignore inter-robot collisions but respect critical manipulable object collisions; (3) deploy a priority-based, decoupled multi-agent search on the collision-annotated roadmaps to efficiently generate optimized, collision-free robot trajectories that fulfill the assembly task plan and task assignments.

This work was supported by Kawasaki Heavy Industry, Ltd (KHI) under grant number 030118-00001. This article solely reflects the opinions and conclusions of its authors and not KHI or any other Kawasaki entity.

[1]Massachusetts Institute of Technology; [2]University of Southern California; [3]University of Illinois Urbana-Champaign; [4]NVIDIA; * indicates equal contributions; Email: jkchen@csail.mit.edu

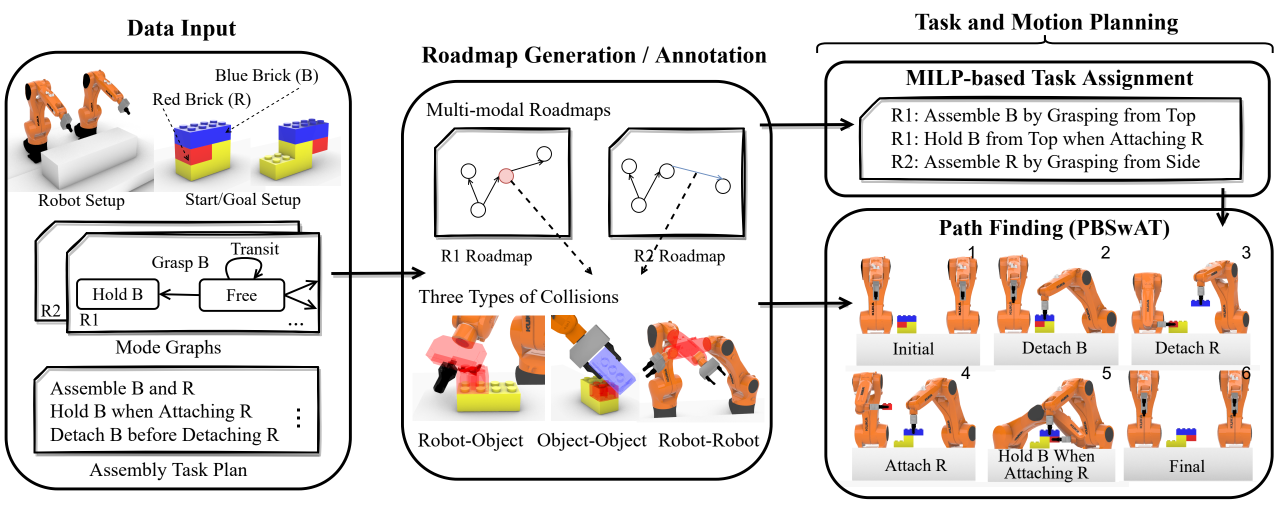

Fig. 1: Phases of the proposed multi-robot task and motion planning algorithm on a two-robot Lego assembly problem.

To demonstrate our planning system's ability to automatically generate optimized assembly solutions for complex assembly structures with multiple robot arms, we test on several challenging simulated assembly domains involving Lego bricks, bars, plates, and irregular-shaped blocks with grippers or suction plates as end-effectors for up to 23 objects.

II. Related Work

Automating the assembly of mechanical parts or spatial structures using programmable robots has been studied from the early days of classic assembly planning [1] to the recent advancements in the robotic assembly of architecture [2] and furniture [3]. For single-robot assembly with a fixed, repetitive motion primitive pattern, such as spatial extrusion and pick-and-place assembly, recent research has proposed scalable planning algorithms to solve sequence and motion planning problems with a large number of components [4], [5]. However, these algorithms are hard to extend to general assembly domains without a pre-assigned, repetitive plan skeleton, especially multi-robot settings. Previous research has proposed planning systems for coordinating multiple robots to assemble furniture [3] and LEGO blocks [6], but these works focus on activity planning aspects with limited consideration in robot motions and thus do not generate collision-free trajectories.

Early attempts in Multi-Modal Motion Planning (MMMP) solve multi-step manipulation problems by planning across the configuration spaces of manipulation modes [7], [8]. Recent works in Task and Motion Planning (TAMP) further bridge symbolic reasoning about actions that achieve desired goals and geometric reasoning in search of a collision-free robotic motions [9]. Research in this area seeks to combine discrete task planning from the Artificial Intelligence (AI) communityand continuous motion planning from the robotic communityto allow reasoning on both levels simultaneously [10]–[12]. Although capable of modeling and solving multi-robot assembly problems [13]–[15], neither MMMP nor TAMP methods take advantage of the factored nature of multi-robot systems and thus are inefficient to plan for a team of robots.

Multi-Agent Path Finding (MAPF) aims at navigating a group of agents, such as vehicles or drones, to reach specified goals without colliding. MAPF algorithms operate on a graph where each agent occupies exactly one vertex and can only move to adjacent vertices at each discretized time step. Recent work in this field significantly improved the scalability of the algorithms [16] and generalized grid-world planning to incorporate task assignment [17], [18]. Conflict-based search originates from MAPF and has been successfully applied to perform multi-arm motion planning [19]. Inspired by the Priority-Based Search (PBS) approach [20], our assembly planning system explores task priorities to generate collision-free paths. In addition to being able to plan for multiple tasks, our system solves a path finding problem on general roadmaps with annotated collisions and continuous traversal time compared to classical MAPF.

III. Problem Formulation

A multi-robot assembly planning problem is defined as the problem of planning control trajectories for a team of robots $A = \{a_1, .., a_N\}$ from their start configurations to manipulate a set of objects $O = \{o_1, ..o_M\}$ such that (1) the robots assemble all the objects with respect to the assembly requirements and finish at their goal configurations, and (2) robots, objects, and obstacles do not collide. We use makespan (i.e., plan execution time) as our optimization criteria. In this paper, we specifically consider planning for robot arms, but our approach can be applied to other multi-robot teams.

In our example in Fig. 1, B and R must be detached from the base and then attached at a new location. During the process, B needs to be held while R is being attached. To describe such assembly requirements, we use mode graphs to qualitatively describe the procedures of the robots manipulating the objects. We use an assembly task plan that leverages this mode graph representation to describe the assembly requirements.

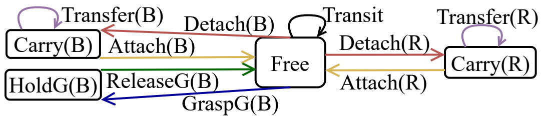

Fig. 2: Mode graph.

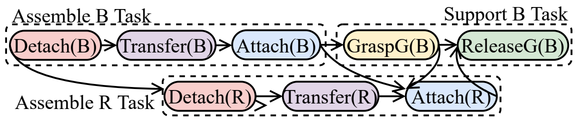

Fig. 3: Assembly task plan.

A. Mode Graphs

A mode graph for a robot $a_n \in A$ is a directed graph $\langle \Sigma_n, \mathcal{T}_n \rangle$: nodes Σ_n are a set of modes that specify a qualitative relation between a_n and objects, each of which represents a set of robot configurations and the manipulated object states, and directed edges $\mathcal{T}_n$ between nodes are motion primitives, each of which represents a set of moving or manipulating trajectories. Thus, a robot trajectory along with the manipulated object states over time can be qualitatively described as a time-stamped, interleaving sequence of modes and primitives.

Fig. 2 shows the mode graph of a robot manipulating B and R in our example: the modes classify the states as free hand (Free), carry an object (Carry), and hold an object at its goal to be stable (HoldG); the primitives classify the trajectories as move with free hand (Transit), transfer an object (Transfer), detach an object from its base or attach it at its target (Detach, Attach), and grasp or release an object at its goal pose (GraspG, ReleaseG).

B. Assembly Task Plans

An assembly task plan is defined as $\langle \mathrm{T}, \mathrm{P} \rangle$: T is a set of tasks, where each task $\mathrm{T}_p = (\tau_{p,1}, .., \tau_{p,K_p}) \in \mathrm{T}$ is a sequence of motion primitives that must be achieved by a unique robot, and P is a set of precedence constraints, and each constraint $p = (a, b) \in P$, where a and b are in the form of $(\tau, \vdash)$ or $(\tau, \dashv)$, represents the start ($\vdash$) or end ($\dashv$) times of τ.

Fig. 3 shows an example assembly task plan. There are three tasks: the first two are assembly tasks with primitives [Detach(B), Transfer(B), Attach(B)] and [Detach(R), Transfer(R), Attach(R)], and the other one is a support task [GraspG(B), ReleaseG(B)]. There are three types of precedence constraints in the example: (1) the precedence constraints between subsequent modes or primitives in the same task (e.g. Detach(B) precedes Transfer(B)); (2) Detach(B) precedes Detach(R), Attach(B) precedes Attach(R), and Attach(B) precedes GraspG(B) given the assembly structure; (3) Attach(R) precedes Grasp(B) and succeeds ReleaseG(B) given the support requirement.

IV. Roadmap Generation

Given a robot a_n and its mode graph $(\Sigma_n, \mathcal{T}_n)$, we generate a multi-modal roadmap $G_n = (\mathrm{V}_n, \mathrm{E}_n)$ to describe its feasible movements and interaction with the objects. Vertices V_n are a set of configurations, and each vertex $v \in \mathrm{V}_n$ is labeled with a mode $v.\sigma$ and, when relevant, a grasp pose $v.\mathrm{p}$ for the currently manipulated object. $v.\mathrm{p} = \emptyset$ if $v.\sigma =$ Free. Directed edges E_n are a set of trajectories, and each edge $e \in \mathrm{E}_n$ from vertex $e.\mathrm{s}$ to vertex $e.\mathrm{e}$ with minimum traversal time $e.\mathrm{w}$ is labelled with a primitive $e.\tau$ and a grasp pose $e.\mathrm{p}$. Let $e.\mathrm{p} = \emptyset$ if $e.\tau =$ Transit. These vertices and edges are collision-free with the robot itself and static obstacles but not necessarily collision-free with dynamic obstacles. Fig. 4 shows an example multi-modal roadmap.

We sample the multi-modal roadmap in a manner similar to the general MMMP sampling method described in [8], which iteratively samples in the mode configuration space and the transition space. Similarly, in our mode graph, the primitives can be classified as mode-changing primitives (e.g., Detach, Attach, GraspG, ReleaseG) and mode-preserving primitives (e.g., Transit, Transfer). As the transition space in assembly problems is structured, we take a task-aware sampling method. The edges and vertices are sampled as follows: (1) we first use manipulation skill simulators to sample a diverse set of trajectories as edges called *mode-changing edges* (i.e., the red, yellow, blue, and green edges in Fig. 4) for mode-changing motion primitives, and their starts and ends are *milestones* of the corresponding modes (e.g., the solid-line circles); (2) then we sample edges and vertices for the mode-preserving primitives and the pointed modes, which also connect the previously sampled milestones. These edges and vertices compose a *single-mode roadmap* of a mode-preserving primitive and its pointed mode (e.g., the black lines and the dashed circles). We have two ways to sample such single-mode roadmaps: (2a) we generate single-mode roadmaps for the other primitives and modes (e.g., Transit-Free roadmap and Transfer-Carry roadmap) by using roadmap spanners [21], which are connected to the milestones; (2b) we can also generate a single-mode roadmap by using RRT-connect [22] to find paths (i.e., an interleaving sequence of edges and vertices) between milestones as *highways*. Vertices in (2a) and (2b) can be connected together via *connection edges* to enhance connectivity. Because roadmap vertices also differ in grasp poses, a single-mode roadmap can have multiple disconnected parts under different relative grasp poses. For example, grasping B from the top or side results in two disjoint components in Carry(B)), which is reflected in Fig.4.

In a multi-modal roadmap, mode-changing edges (step 1) and highways (step 2b) are enough to capture the fastest paths for a robot to complete tasks while the spanned vertices and edges (step 2a) can serve as alternatives when the highways are blocked by other robots during a time window. Thus, to reduce the roadmap size, we sample and add these edge differently for task assignment and path finding. In task assignment, since we only consider inter-robot collisions of mode-changing edges, we use a multi-modal roadmap only consisting of mode-changing edges and highways. Then, when the tasks are assigned, we use a multi-modal roadmap consisting of all the spanned vertices and edges and the highways that are related to the assigned tasks, which are connected via corresponding

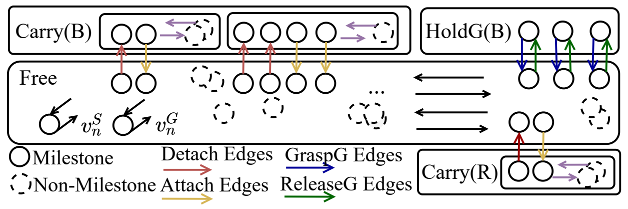

Fig. 4: Multi-modal roadmap (most edges in single-mode roadmaps such as Transit-Free and Trasnfer-Carry are omitted).

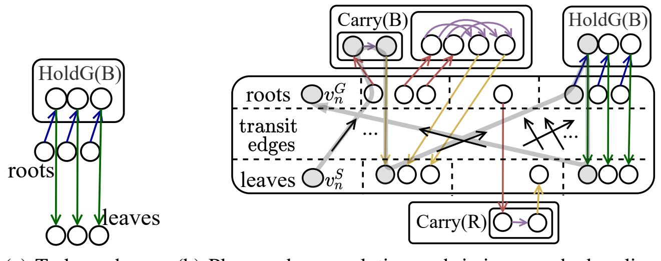

(a) Task roadmap (b) Plan roadmap: solution path is in gray shadow line

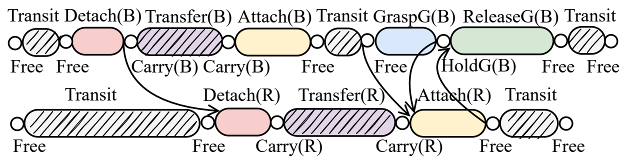

(c) Subplan sequences: nodes denote modes and blocks denote primitives

Fig. 5: Task roadmap, plan roadmap, and subplan sequences.

connection edges. As each object has a unique Carry-Transfer roadmap, the numbers of spanned vertices and edges increase linearly with the object number. Thus, to further reduce the generation time, we cache the arm configurations and collision checking information in the Transit-Free roadmap and reuse them for spanning other single-mode roadmaps in the same multi-modal roadmap. As a result, a large portion of spanned components share the same arm configurations.

A. Collision Annotation

Although a robot and its manipulated object are guaranteed to be collision-free with the obstacles when traversing through its roadmap, they also need to avoid colliding with other moving robots and objects to be safe. We adopt the idea of annotated collisions Π in [23] to characterize pairwise collisions between robot and robot, robot and object, or object and object in our assembly problem. Each annotated collision $\pi \in \Pi$ is a pair of conditions, where each condition denotes an area swept by a robot or an object in the workspace, and the annotated collision implies that the two areas of the conditions overlap. Specifically, in our problem, we have two types of conditions: (1) edge condition (a_n, e) and vertex condition (a_n, v) represent the swept area of robot a_n and its manipulated object when traversing edge $e \in \mathrm{E}_n$ or waiting at vertex $v \in \mathrm{V}_n$; (2) object condition $(o_m, \perp)$ or $(o_m, \top)$ represent the area occupied by object o_m being at its start $(\perp)$ or goal position $(\top)$, respectively. With all the roadmaps, we collect the conditions for all the robots and objects. Then, we do pairwise collision checks between them to record the colliding pairs as annotated collisions. As a large portion of vertices and edges in a multi-modal roadmap share the same arm configurations, they sweep the same area and the collisions between them and others are only checked once.

V. Task Assignment

The task assignment module is to generate an optimal plan in which each robot takes a sequence of tasks such that all assembly tasks are assigned with respect to the assembly requirements and roadmap connectivity. The optimizing criteria is minimizing the makespan. The task assignment problem at this stage is a relaxation of the original problem since we ignore potential collisions when robots traverse through non-milestones. Fully collision-free paths will be generated by our multi-task multi-agent path finding algorithm by refining a set of partially ordered subplans extracted from our task assignment solution (Section VI). This problem can be treated as an extension of Vehicle Routing Problems with Time Windows with exclusion constraints [24] and formulated as a Mixed Integer-Linear Program (MILP) [17].

1) Task Roadmap: For every task $\mathrm{T}_p = (\tau_{p,1}, .., \tau_{p,K_p}) \in \mathrm{T}$ and every robot a_n, we extract *task roadmap* $\mathrm{G}^{\mathrm{T}}_{n,p}$, an acyclic directed graph that represents all the paths of a_n to complete task T_p. We construct $\mathrm{G}^{\mathrm{T}}_{n,p}$ by (1) collecting all the milestones and mode-changing edges introduced by primitives T_p to G_n; and (2) in each mode, adding a mode-preserving edge from every milestone that ends a mode-changing edge to every milestone that starts an mode-changing edge with the minimum traversal time as the weight except for mode Free. The added edge is an abstraction of the highways between milestones and thus has the same primitive. A task roadmap example is given in Fig.5(a).

2) Plan Roadmap: Then, given all the tasks T, we construct a *plan roadmap* $\mathrm{G}^{\mathrm{T}}_n$ for every robot a_n to represent all the paths of a_n to complete tasks T. To construct $\mathrm{G}^{\mathrm{T}}_n$, we first compose all the task roadmaps $\otimes_p \mathrm{G}^{\mathrm{T}}_{n,p}$. We find the root vertices of all the task roadmaps along with the robot goal vertex as the plan roots, and the leaf vertices along with the robot start vertex as the plan leaves. Roots and leafs have zero in-degree and out-degree, respectively. Then, we add an edge from every leaf to every root with its minimal traversal time except the vertices belonging to the same task roadmap. The nodes of this plan roadmap are not necessarily the subset of the multi-modal roadmap since some tasks are required to execute more than once. An example of plan roadmap is given in Fig.5(b).

3) MILP Encoding: For every $a_n \in A$ and every edge $e \in \mathrm{G}^{\mathrm{T}}_n.\mathrm{E}$, we have a binary variable $A[e]$ to indicate that a_n traverses edge e and a non-negative real variable $t_n[v]$ to denote the times of a_n arriving $v \in \mathrm{G}^{\mathrm{T}}_n.\mathrm{V}$. For every primitive $\tau_{p,k} \in \mathrm{T}_p$, we use real variables $t_{\mathrm{T}}[\tau_{p,k}, \vdash]$ and $t_{\mathrm{T}}[\tau_{p,k}, \dashv]$ to denote the start and end times of $\tau_{p,k}$, respectively. By slightly abusing the notation, we also use $t_{\mathrm{T}}[e.\mathrm{s}]$ and $t_{\mathrm{T}}[e.\mathrm{e}]$ to denote the same variables as $t_{\mathrm{T}}[\tau_{p,k}, \vdash]$ and $t_{\mathrm{T}}[\tau_{p,k}, \dashv]$ for $e \in \mathrm{G}^{\mathrm{T}}_n.\mathrm{E}$ if e is labeled with $\tau_{p,k}$. We use real variable t to denote the total makespan. For a vertex $v \in \mathrm{G}^{\mathrm{T}}_n$, we denote its incoming edges in $\mathrm{G}^{\mathrm{T}}_n$ as $\textsc{in}(v)$ and the outgoing edges as $\textsc{out}(v)$. The implication logic in the MILP model is compiled to linear constraints by using the big-M method.

minimize t

$$\textstyle\sum_{e \in \textsc{in}(v)} A[e] = \sum_{e \in \textsc{out}(v)} A[e], \qquad \forall v \in \cup_n \mathrm{G}^{\mathrm{T}}_n.\mathrm{V}/\{v^{\mathrm{S}}_n, v^{\mathrm{G}}_n\} \tag{1}$$

$$\textstyle\sum_{e \in \textsc{out}(v)} A[v^{\mathrm{S}}_n] = 1, \sum_{e \in \textsc{in}(v)} A[v^{\mathrm{G}}_n] = 1, \qquad \forall n \in (1..N) \tag{2}$$

$$A[e] \rightarrow (t_n[e.\mathrm{e}] - t_n[e.\mathrm{s}] \geq e.\mathrm{w}), \qquad \forall e \in \cup_n \mathrm{G}^{\mathrm{T}}_n.\mathrm{E} \tag{3}$$

$$\textstyle\sum_{e \in \mathrm{E}} A[e] = 1, \qquad \forall \mathrm{T}_{k,p} \in \mathrm{T} \text{ where } \mathrm{E} = \cup_n G^{\mathrm{T}}_{n,p,k}.\mathrm{E} \tag{4}$$

$$A[e] \rightarrow (t_{\mathrm{T}}[e.\mathrm{s}] = t[e.\mathrm{s}])) \wedge (t_{\mathrm{T}}[e.\mathrm{e}] = t[e.\mathrm{e}])), \qquad \forall e \in \mathrm{G}^{\mathrm{T}}_n.\mathrm{E} \tag{5}$$

$$t_{\mathrm{T}}[a] \leq t_{\mathrm{T}}[b], \qquad \forall (a,b) \in \mathrm{P} \text{ and } (t \geq t_n[\cdot] \wedge t \geq t_{\mathrm{T}}[\cdot]) \tag{6}$$

$$(A[e] \wedge A[e']) \rightarrow (t_n[e.\mathrm{e}] < t_{n'}[e'.\mathrm{s}]) \vee (t_{n'}[e'.\mathrm{e}] < t_n[e.\mathrm{s}])),$$
$$\forall ((a_n, e), (a_{n'}, e')) \in \Pi \text{ and } e \in G_n, e' \in G_{n'} \tag{7}$$

$$A[e] \rightarrow (t_n[e.\mathrm{s}] > t_{\mathrm{T}}[\tau, \vdash]), \quad \forall ((a_n, e), (o, \perp)) \in \Pi, \forall \tau \text{ detaches } o \tag{8}$$

$$A[e] \rightarrow (t_n[e.\mathrm{e}] < t_{\mathrm{T}}[\tau, \dashv]), \quad \forall ((a_n, e), (o, \top)) \in \Pi, \forall \tau \text{ attaches } o \tag{9}$$

While constraints (1-2) ensure every robot a_n traverse through a valid path in its plan roadmap G^{T}_n from its start v^{S}_n to goal v^{G}_n, (3) enforces the arrival time of the vertices on this path to respect the traversal time. Then, (4) constrains each task to be assigned to exactly one robot, and (5) links the start and end times of each task primitive with the arrival times of its assigned robot. (6) enforces these start and end times to satisfy the precedence constraints P provided in the task plan, and makespan t is the upper bound of all the time variables. Thus, constraints (1-6) ensure all the tasks are taken by exactly one robot while optimizing the total execution time.

We also add constraints (7-9) to prevent robots from colliding with objects or each other when taking mode-changing edges, which are often the manipulation action and can easily lead to deadends given the intricate assembly structure. Constraint (7) enforces the mode-changing edges that collide with each other not to happen concurrently, and (8) guarantees such edges that collide with objects at starts or goals are not taken before detaching or after attaching objects, respectively.

4) Extracting Subplan Sequences: Given a MILP solution of each robot as the gray shadow path in Fig.5(b), we can extract a *subplan sequence* $\gamma_n = \{g_{n,k}\}_k$ for this robot as shown in Fig. 5(c). Each subplan is a mode or primitive associated with the start and end vertices as assigned in the MILP solution. Thus, the end and start of two subsequent subplans are the same vertex. A subplan $g_{n,k}$ is *planned* if a time-stamped path from its start vertex to its end vertex on roadmap G_n is provided. The subplans can be classified as three types: (1) a mode subplan has identical start and end vertices and thus its path is a single vertex; (2) implicitly, the path of a mode-changing primitive subplan can only traverse its corresponding edge in the MILP solution; and (3) the other primitive subplans need more efforts to plan longer paths such as Transit and Transfer primitives as sketched in Fig. 5(c). We extract such subplan sequences for all robots to obtain $\Gamma = \{\gamma_n\}_n$ and add precedence constraints $\mathcal{P}$ between the subplan end times according to the assembly task plan, which together are the goal description of our collision-free pathfinding algorithm introduced in Section VI.

Algorithm 1: PBSwAT
```
1  $Root = (paths, C, \prec) \leftarrow (\emptyset, \emptyset, \mathcal{P})$;
2  $S \leftarrow \{Root\}$;
3  while $(N \leftarrow S.pop()) \neq \emptyset$ do
4      while $\mathcal{C}_N = \emptyset$ do
5          if $g_i \leftarrow NextUnplannedSubplan(\prec_N)$ is false then
6              return $N.paths$;
7          if $paths \leftarrow PlanPaths(N, g_i)$ is false then
8              go to Line 3;
9          foreach $p_i \in paths$ do $N.paths[g_i] \leftarrow p_i$;
10         $\mathcal{C}_N \leftarrow UpdateCollisions(N, paths)$;
11     $g_i, g_j \leftarrow$ two subplans involved in the 1st collision in $\mathcal{C}_N$;
12     foreach $(g_k, g_l) \in \{(g_i, g_j), (g_j, g_i)\}$ do
13         $N' \leftarrow (N.paths, \mathcal{C}_N, \prec_N \cup \{g_k \prec g_l\})$ ;
14         if UpdateNode$(N', g_k)$ is true then $S.insert(N')$;
15 return false;
```

VI. Path Finding with Assigned Tasks

We now introduce our Priority-Based Search algorithm for multi-robot pathfinding with Assigned Tasks, denoted as PBSwAT, that plans paths for every robot a_n to fulfill its subplan sequence γ_n on its multi-modal roadmap G_n such that the precedence constraints $\mathcal{P}$ are satisfied and the paths are collision-free given annotated collision Π. The idea of PBSwAT is to divide a multi-robot problem into single-robot sub-problems and explore the priorities of planning sub-problems as proposed in Priority-Based Search (PBS) [20]. PBS is a two-level algorithm that plans collision-free paths for multiple robots from their starts to goals in grid graphs (i.e., classical MAPF). As its high level explores the priorities between robots in a Priority Tree (PT) such that lower-priority robots should avoid colliding with higher-priority robots, its low level uses A* to plan single-robot paths optimally in discretized timesteps by reserving the paths of higher-priority robots as moving obstacles. While PBSwAT is also a two-level algorithm similar to PBS, its high level explores the priorities between subplans instead of robots and calls its low level to plan paths for subplans lazily instead of calling it to plan all the paths at the beginning, and its low level plans paths for multiple successive same-robot subplans at once instead of one subplan at a time. For simplicity, in this section, we use g_i, $i = 1, \ldots, \sum_{a_n \in A} |\gamma_n|$, instead of $g_{n,k}$ to denote a subplan, where subplans of different robots have different index values i, and p_i to denote its corresponding path.

The high level of PBSwAT (Algorithm 1) performs a depth-first search on the PT. It starts with the root PT node that contains an empty set of paths, an empty set of collisions, and the initial priority orderings $\prec$, which are initialized with respect to the precedence constraints $\mathcal{P}$ to enforce the subplans that must end later to have lower priorities (Line 1). The

Algorithm 2: UpdateNode (PT node N, subplan g_i)

```
1  $R \leftarrow \{g_i\}$;    // sort subplans to replan in in order of $\prec_N$
2  while $(g_j \leftarrow R.pop()) \neq \emptyset$ do
3      if livelock occurs then return false;
4      if $paths \leftarrow$ PlanPaths$(N, g_j)$ is false then return false;
5      foreach $p_k \in paths$ do $N.paths[g_k] \leftarrow p_k$;
6      $R \leftarrow R \cup \{g_l \mid (g_k \prec_N g_l) \wedge (g_k, g_l) \in \mathcal{C}_N, p_k \in paths\} \cup \{g_l \mid$
         $g_k$ precedes $g_l) \wedge (N.paths[g_l].T < p_k.T), p_k \in paths\}$;
7      $R \leftarrow R \setminus \{g_k \mid p_k \in paths\}$;
8  return true;
```

precedence constraints between subsequent same-robot subplans are trivially included. Then, a stack S is initialized with the root node (Line 2). When expanding PT node N (Line 3), it first plans paths for unplanned subplans one at a time with respect to the priority orderings $\prec_N$ (Lines 4 to 10), i.e., *NextUnplannedSubplan* always returns the unplanned subplan that does not have any unplanned higher-priority subplans (Line 5), until (1) some collisions are found (Line 4), (2) all paths are planned, in which case we return the paths (Line 6), or (3) no paths exist, in which case we prune N (Line 8). *PlanPaths*(N, g_i) returns a set of paths because it plans a path for g_i and, if necessary, replans paths for the previous same-robot subplans of g_i. More details of these subroutines will be introduced below. Last, PBSwAT resolves a collision in $\mathcal{C}_N$ in the same way as PBS and replans the paths in each generated child node by calling *UpdateNode* (Lines 11 to 14).

UpdateNode (Algorithm 2) iteratively updates the paths of all the affected lower-priority subplans until all planned paths in *N.paths*: (1) satisfy the precedence constraints, (2) do not collide with any objects, and (3) any two planned paths that have priorities in between are collision-free. It first constructs a priority queue R to store all the subplans to replan, in which subplans are sorted according to $\prec_N$ (Line 1). It then repeatedly calls *PlanPaths* to replan until no more subplans need to be replanned (Line 2), a live lock occurs (Line 3), or a failure is reported by *PlanPaths* (Line 4). A live lock refers to a condition where updating a set of subplans triggers replanning of each other in a loop and leads to infinite replanning. In each iteration, when *PlanPaths* replans paths successfully, PBSwAT updatea *N.paths* accordingly (Line 5), adds the lower-priority subplans that either violate the precedence constraints due to the updated times of the replanned subplans or collide with the updated paths to R (Line 6), and deletes the subplans that have been replanned in this iteration from R (Line 7).

PlanPaths(N, g_i) plans an optimal path for g_i that (1) avoids collisions with the objects and the paths of higher-priority subplans; and (2) ends after the end time of any subplan that must end earlier than g_i. In the case that the subsequent same-robot subplans of g_i already have paths, *PlanPaths* replans their paths accordingly to avoid disjoining the paths of two subsequent subplans over time. Moreover, if there does not exist a path for g_i or its subsequent subplans, *PlanPaths* backtracks and replans the previous subplan of g_i. This backtracking procedure is repeated until *PlanPaths* successfully

Algorithm 3: rSIPP(PT node N,subplan g_i, time t_0, RT rt_i)

```
1  $T_{\min} \leftarrow \max\{N.paths[g_j].T \mid g_j \in \Gamma$ should precede $g_i\}$;
2  generate root node at $g_i.start$ at time $t_0$ and insert it to $Q$;
3  while $(n \leftarrow Q.pop()) \neq \emptyset$ do
4      if $n.v = g_i.goal \wedge n.I.ub > T_{\min}$ then
5          $p \leftarrow$ extract the path from $n$;
6          if $p.T < T_{\min}$ then
7              Add a wait action till time $T_{\min}$ to the end of $p$;
8          $g_j \leftarrow$ the subsequent subplan of $g_i$;
9          if $g_j$ doesn't exist or $N.paths[g_j] = \emptyset$ then return $\{p\}$;
10         $rt_j \leftarrow$ ReservationTable$(N, g_j)$;
11         foreach $[lb, ub) \in rt_j$.SafeIntervals$[n.v]$ do
12             if $([lb', ub') \leftarrow [lb, ub) \cap [p.T, n.I.ub)) \neq \emptyset$
                 $\wedge (paths \leftarrow rSIPP(N, g_j, lb', rt_j)) \neq \emptyset$ then
13                 Add a wait action till time $lb$ to the end of $p$;
14                 return $\{p\} \cup paths$;
15     expand node $n$ w.r.t. $rt_i$ and insert its child nodes to $Q$;
16 return $\emptyset$;
```

finds paths for all the subplans that it has to plan, in which case it returns *true*, or no more previous subplan exists, in which case it returns *false*. In each backtracking iteration with newly added subplan g_j, *PlanPaths* calls recursive SIPP (rSIPP) with g_j, and rSIPP will plan paths for g_j and all its subsequent same-robot subplans that already have paths.

Safe Interval Path Planning (SIPP) [25] is a variant of A* that finds an optimal path in continuous time that avoids given moving obstacles. We adapt it to rSIPP (Algorithm 3) so that it finds a set of paths for successive subplans that avoid the moving obstacles, i.e., the objects and the higher-priority subplans, and satisfies the precedence constraints. It takes input a Reservation Table (RT) as in SIPP that reserves the time intervals at each vertex that are occupied by the moving obstacles. The unreserved time intervals are called safe intervals. rSIPP searches in the resulting vertex-safe-interval graph to find an optimal path that (1) visits each vertex within a safe interval, (2) does not collide with any moving obstacles when it traverses an edge, and (3) ends no earlier than $T_{\min}$, where $T_{\min}$ is the minimum allowable time to finish this subplan with respect to all the subplans that should precede it (Line 1). Its search procedure is the same as that of SIPP except for the goal test. When rSIPP finds a goal node (Line 4), it extracts the path p from n (Lines 5 to 7), checks whether g_i is the last subplan to replan (Lines 8 to 9), and terminates if so; otherwise, it plans for the subsequent subplan g_j to ensure a path starting from the end of p exists (Lines 10 to 14). Specifically, it checks each reachable safe interval at the end vertex with respect to the RT for g_j, calls rSIPP for each of them, and, if succeed, returns the found paths together with p.

VII. Experimental Results

In our implementation of roadmap generation and collision annotation, we leverage PyBullet Planning to generate single-mode roadmaps, check collision, and simulate skill trajectories[1]. We ran the MILP encodings for task assignment by using

[1]https://pypi.org/project/pybullet-planning/

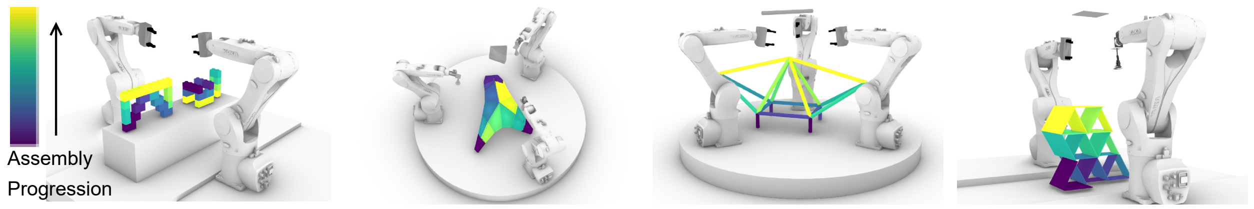

(a) Lego Bridge (b) Puzzle Vault (c) Truss Boat (d) Card House

Fig. 6: Problem instances. (a) Lego Bridge: two robots with grippers assemble 17 Lego bricks; (b) Puzzle Vault: three robots with suction plates assemble 14 irregular-shaped blocks; (c) Truss Boat: three robots with grippers assemble 16 bars; (d) Card House: two robots with gripper and suction plates assemble 23 plates.

Domain	Roadmap Generation & Annotation				MILP-based Task Assignment				PBSwAT				
	$\#V$	$\#E$	t_{map}(min)	t_{anno}(hr)	#B	#X	#C	$t_T/t_T^\dagger/t_T^*$(s)	$\#g$	#N	#rSIPP	t_P(s)	η
Lego Bridge	8450	13454	87	741	2985	83	95795	40/44/65	166	6	214	66	0.04
Puzzle Vault	4973	8642	103	1289	1148	57	2853	3/10/11	129	29	278	32	0.22
Truss Boat	4049	8688	86	1035	18857	88	51224	90/175/496	153	44	221	122	0.18
Card House	8188	12818	112	861	4253	141	13157	71/105/821	190	11	221	17	0.03

TABLE I: Experimental Results. $\#V/\#E$: average vertex/edge number of highways and connections; t_{map}: average roadmap generation time; t_{anno}: roadmap annotation time; #B,#X,#C: number of binary variables, continuous variables, and constraints in the MILP; t_T,$t_T^\dagger$,t_T^*: runtimes to find a feasible MILP solution, find an optimal solution, and exhaust the solution space; #g: number of subplans; #N: number of expanded nodes; #rSIPP: calls to rSIPP; t_P: PBSwAT runtime; η: ratio of the used annotated collisions.

Gurobi [26]. The PBSwAT algorithm is implemented in C++. We execute most our implementation on a 3.40GHZ 8-Core Intel Core i7-6700 CPU with 36GB RAM and leverage 100 CPUs each with 8G memory on Amazon Web Service (AWS) to parallel compute annotated collisions. In all the domains, We use Kuka KR-6-R900 arms with grippers or suction plates.

We generate 500 vertices for the Free-and-Transit single-mode roadmap by using the k-nearest PRM with $k = 10$. This generation takes roughly 40 minutes in all the domains. The maximum sample number of RRT-connect is set to 3000. The highway vertices are connected to its 20 nearest spanned vertices via connection edges. The maximum edge duration is 0.1s, and longer edges are interpolated to sequences of edges. The robot joint resolution for collision checking is set to 0.01π.

We test our examples on domains with different features as shown in Fig. 6: (a) Lego Bridge: two robots with grippers need to detach 17 Lego bricks from the right and assembly them as a bridge, during which necessary holding actions are provided to keep Lego bricks stable; (2) Puzzle Vault: three robots with suction plates assembly a vault with 14 irregular-shaped blocks; (3) Truss Boat: three robots with grippers assemble a bridge with 16 bars in a narrow space; (4) Card House: two robots with a gripper and a suction plate, respectively, cooperate to assemble a construction with 23 plates together, in which our planner should be aware of different robot abilities such as only the robot with the suction plate can place plates at the bottom. In the last three domains, we assume objects are teleported to the top of the construction for robots to pick. All the domains are borrowed from the real-world designs and the assembly task plans are extracted given the design structure. The simulations are provided in the supplementary materials.

The runtime results and statistics of each step (Section IV, V, VI) are reported in TABLE I. For roadmap generation and annotation, we only report the generation time of the roadmaps that are used by PBSwAT and skip the statistics for the roadmap used by task assignment. The latter roadmap of each robot is of a much smaller size and takes less than 20 minutes to generate and annotate. We report the average number of sampled vertices and edges for highways and connection edges over all the robots (#V, #E). We do not include the size of the whole multi-modal roadmap in this section. Because the Transfer-Carry roadmaps share a large portion of same arm configurations as the previously sampled Transit-Free roadmaps, and the highways and connection edges are more representative to the problem sizes of different domains. We also report the runtime to generate this multi-modal roadmap (t_{map}), and the runtime to annotate all the necessary collision pairs (t_{anno}). They also include the time to generate and annotate the shared configurations in Transit-Free roadmaps. As we can see in the table, the time to generate roadmaps is around 100 minutes for each robot and the annotation time can be around 1000 hours. Although we leverage CPU clusters for parallel computation and reduce the total runtime to a couple of hours, this time can be significantly reduced by using (1) lazily roadmap generation and annotation methods [27], [28]; or (2) Voxel-based collision checking by using GPUs [29]. We consider implementing these techniques into our planning systems as important future work.

In the MILP-based task assignment, we report the numbers of binary variables (#B), continuous variables (#X), and constraints (#C) along with the runtimes to find the first solution t_T, find the optimal solution $t_T^\dagger$, and exhaust the solution space t_T^*. As we can see in the table, all the MILP encodings feature a relatively small number of continuous variables and can have up to eighteen thousand binary variables. #B is dominated by the number of mode-changing edges and the potential collision between these edges. Thus, we can see Truss Boat has the largest #B since its mode-changing edges are very easy to collide with each other or the objects. Although these MILPs are of huge size, Gurobi can find a feasible solution in two minutes and then an optimal one in a couple of minutes for all the domains, which is due to the relatively small number of continuous variables in all the domains.

In the PBSwAT column, we show the number of all the subplans (#g), the expanded nodes (#N), the calls to rSIPP (#rSIPP), the runtime to find the solutions (t_P), and the ratio of the used annotated collisions over all the annotated collisions (η). As we can see, all the domains can be solved in two minutes with few expansions up to 44 times. We also observe that, in crowded domains such as Puzzle Vault and Truss Boat, in which robots are easy to collide above the structure, PBSwAT needs to expand more nodes and add more priorities, and η can be up to 22%. However, in the setups where robots are front to front and do not collide often, η can be low as 3%. As we can see, our task assignment and path finding algorithms can quickly find high-quality solutions in a couple of minutes, the overall runtime is dominated by roadmap generation and collision annotation.

VIII. Conclusion and Future Work

In this paper, we present a cooperative task and motion planner that jointly plans safe, optimized assembly plans for multiple robot arms to assemble complex structures. We demonstrate its capabilities in several challenging domains. The future work includes (1) improving the implementation of roadmap generation and annotation by using GPU-based collision checking and lazy roadmap generation; and (2) adjusting task assignments online in PBSwAT.

References

[1] R. H. Wilson, "On Geometric Assembly Planning." Ph.D. dissertation, Stanford University, 1992.

[2] Y. Huang, L. P. Y. Victor, C. Garrett, F. Gramazio, M. Kohler, and C. Mueller, "The new analog: A protocol for linking design and construction intent with algorithmic planning for robotic assembly of complex structures," in *Symposium on Computational Fabrication*, ser. SCF '21. Association for Computing Machinery, 2021.

[3] R. A. Knepper, T. Layton, J. Romanishin, and D. Rus, "Ikeabot: An autonomous multi-robot coordinated furniture assembly system," in *2013 IEEE International conference on robotics and automation*. IEEE, 2013, pp. 855–862.

[4] C. R. Garrett, Y. Huang, T. Lozano-Pérez, and C. Mueller, "Scalable and probabilistically complete planning for robotic spatial extrusion," in *Robotics: Science and Systems XVI, Virtual Event / Corvalis, Oregon, USA, July 12-16, 2020*, 2020.

[5] Y. Huang, C. Garrett, I. Ting, S. Parascho, and C. Mueller, "Robotic additive construction of bar structures: Unified sequence and motion planning," *Construction Robotics*, 2021.

[6] L. Nägele, A. Hoffmann, A. Schierl, and W. Reif, "Legobot: Automated planning for coordinated multi-robot assembly of lego structures," in *IEEE/RSJ Intl. Conf. on Intell. Robots and Systems*, 2020.

[7] K. Hauser and V. Ng-Thow-Hing, "Randomized multi-modal motion planning for a humanoid robot manipulation task," *The International Journal of Robotics Research*, vol. 30, no. 6, pp. 678–698, 2011.

[8] K. Hauser and J.-C. Latombe, "Multi-modal motion planning in non-expansive spaces," *The International Journal of Robotics Research*, vol. 29, no. 7, pp. 897–915, 2010.

[9] C. R. Garrett, R. Chitnis, R. Holladay, B. Kim, T. Silver, L. P. Kaelbling, and T. Lozano-Pérez, "Integrated Task and Motion Planning," *Annual review of control, robotics, and autonomous systems*, vol. 4, 2021.

[10] C. R. C. Garrett, T. Lozano-Pérez, and L. L. P. Kaelbling, "Sampling-based methods for factored task and motion planning," *The International Journal of Robotics Research*, vol. 37, no. 13-14, 2018.

[11] S. Srivastava, E. Fang, L. Riano, R. Chitnis, S. Russell, and P. Abbeel, "Combined Task and Motion Planning Through an Extensible Planner-Independent Interface Layer," in *IEEE International Conference on Robotics and Automation (ICRA)*, 2014.

[12] M. Toussaint, "Logic-geometric programming: an optimization-based approach to combined task and motion planning," in *IJCAI International Joint Conference on Artificial Intelligence*. AAAI Press, 2015, pp. 1930–1936.

[13] M. Toussaint and M. Lopes, "Multi-bound tree search for logic-geometric programming in cooperative manipulation domains," in *Proceedings - IEEE International Conference on Robotics and Automation*, 2017, pp. 4044–4051.

[14] J. Motes, R. Sandström, H. Lee, S. Thomas, and N. M. Amato, "Multi-Robot Task and Motion Planning With Subtask Dependencies," *IEEE Robotics and Automation Letters*, vol. 5, no. 2, pp. 3338–3345, 2020.

[15] V. N. Hartmann, A. Orthey, D. Driess, O. S. Oguz, and M. Toussaint, "Long-Horizon Multi-Robot Rearrangement Planning for Construction Assembly," *arXiv preprint arXiv:2106.02489*, 2021.

[16] A. Felner, R. Stern, S. E. Shimony, E. Boyarski, M. Goldenberg, G. Sharon, N. Sturtevant, G. Wagner, and P. Surynek, "Search-based optimal solvers for the multi-agent pathfinding problem: Summary and challenges," in *Tenth Annual Symposium on Combinatorial Search*, 2017.

[17] K. Brown, O. Peltzer, M. A. Sehr, M. Schwager, and M. J. Kochenderfer, "Optimal sequential task assignment and path finding for multi-agent robotic assembly planning," in *2020 IEEE International Conference on Robotics and Automation (ICRA)*. IEEE, 2020, pp. 441–447.

[18] W. Hönig, S. Kiesel, A. Tinka, J. Durham, and N. Ayanian, "Conflict-based search with optimal task assignment," in *Proceedings of the International Joint Conference on Autonomous Agents and Multiagent Systems*, 2018.

[19] I. Solis, J. Motes, R. Sandström, and N. M. Amato, "Representation-optimal multi-robot motion planning using conflict-based search," *IEEE Robotics and Automation Letters*, vol. 6, no. 3, pp. 4608–4615, 2021.

[20] H. Ma, D. Harabor, P. J. Stuckey, J. Li, and S. Koenig, "Searching with consistent prioritization for multi-agent path finding," in *Proceedings of the AAAI Conference on Artificial Intelligence*, vol. 33, no. 01, 2019, pp. 7643–7650.

[21] L. E. Kavraki, P. Svestka, J.-C. Latombe, and M. H. Overmars, "Probabilistic roadmaps for path planning in high-dimensional configuration spaces," *IEEE transactions on Robotics and Automation*, vol. 12, no. 4, pp. 566–580, 1996.

[22] J. J. Kuffner and S. M. LaValle, "Rrt-connect: An efficient approach to single-query path planning," in *Proceedings 2000 ICRA. Millennium Conference. IEEE International Conference on Robotics and Automation. Symposia Proceedings (Cat. No. 00CH37065)*, vol. 2. IEEE, 2000, pp. 995–1001.

[23] W. Hönig, J. A. Preiss, T. S. Kumar, G. S. Sukhatme, and N. Ayanian, "Trajectory planning for quadrotor swarms," *IEEE Transactions on Robotics*, vol. 34, no. 4, pp. 856–869, 2018.

[24] G. Laporte and I. H. Osman, "Routing problems: A bibliography," *Annals of operations research*, vol. 61, no. 1, pp. 227–262, 1995.

[25] M. Phillips and M. Likhachev, "Sipp: Safe interval path planning for dynamic environments," in *2011 IEEE International Conference on Robotics and Automation*. IEEE, 2011, pp. 5628–5635.

[26] I. Gurobi Optimization, "Gurobi optimizer reference manual," *URL http://www. gurobi. com*, 2021.

[27] R. Bohlin and L. E. Kavraki, "Path planning using lazy prm," in *Proceedings 2000 ICRA. Millennium Conference. IEEE International Conference on Robotics and Automation. Symposia Proceedings (Cat. No. 00CH37065)*, vol. 1. IEEE, 2000, pp. 521–528.

[28] S. Li and J. A. Shah, "Safe and efficient high dimensional motion planning in space-time with time parameterized prediction," in *2019 International Conference on Robotics and Automation (ICRA)*. IEEE, 2019, pp. 5012–5018.

[29] O. S. Lawlor and L. V. Kalée, "A voxel-based parallel collision detection algorithm," in *Proceedings of the 16th international conference on Supercomputing*, 2002, pp. 285–293.